Microstructure Development during Dissimilar Welding: Case of Laser Welding of Ti with Ni involving Intermetallic Phase Formation

S. Chatterjee, T.A. Abinandanan, K. Chattopadhyay

Department of Metallurgy, Indian Institute of Science, Bangalore 560012, India

Abstract

Development of solidification microstructure in a laser welded Ti/Ni dissimilar binary couple is presented. At the fusion interfaces in both Ti and Ni, growth of the base metal grains into the weld pool is inhibited by the presence of composition gradients in the melt. Ti_2Ni dendrites grow *toward* the base metal at the Ti fusion interface. In the Ni side, appearance of a nickel solid solution phase is followed by layers of Ni_3Ti, Ni_3Ti+NiTi eutectic, and NiTi. NiTi dendrites and Ti_2Ni constitute the microstructure in the middle of the weld. Isolated titanium dendrites are observed throughout the weld, but their preferential occurrence toward the top surface of the weld is more prominent. Results are rationalised on the basis of interplay of the transport processes in the weld with the thermodynamics of the Ti-Ni system.

Keywords: Dissimilar welding, Solidification microstructure, Ti-Ni system

1. Introduction

Dissimilar metal welding (DMW) is qualitatively different from similar metal welding (SMW) for the following reasons: (1) thermo-physical properties of the base metals are, in general, different, and this difference can influence the heat transfer during welding; (2) composition becomes a parameter that can vary over a wide range across the weld pool (from 0 to 1 for a binary couple) and consequently, there does not exist a single liquidus isotherm that defines the solid-liquid interface as it does in SMW; (3) nucleation of the phases assumes importance, especially when intermetallic compounds are present in the phase diagram; and (4) in addition to the surface energy driven Marangoni convection, a strong solutal natural convection also can arise when the base metal densities differ significantly. Although SMW is relatively well understood with respect to the fundamentals of the solidification theory (please see, for example, [1], for a comprehensive review), the understanding of solidification of dissimilar welds is made difficult by the complex interaction of these additional factors.

A number of studies [2-12] on DMW have been carried out on systems involving dissimilar grades of steel, *e.g.*, austenitic stainless steels and ferritic/plain carbon steels. Joining of non-ferrous dissimilar couples also has been investigated by some authors [13-19]. These studies were focused mainly on the weldability and weld design aspects of DMW and they also demonstrated the effect of welding variables on the properties of the weld. However, investigations aimed at understanding the effects of the distinguishing aspects of DMW mentioned in the beginning on the solidification of the weld have been fewer. The effect of a drastically different melt composition on the growth of the base metal grains into the weld pool and nucleation of other phases have been noted in some of the studies [6,20,21]. The effect of

asymmetric heat transfer on the development of the weld pool, and the effect of Marangoni convection on the mixing pattern in the weld pool have also been analysed using Computational fluid dynamics models [22, 23]. The study on laser welding of Cu-Ni [22] showed that melting begins and progresses to a larger extent in the Ni side due to its lower thermal diffusivity compared to Cu. Melting of Cu occurred mainly by the convective heat transfer to this side by the Marangoni flow. The computed weld pool shape and the species mixing patterns were found to be in fairly good agreement with the experimental results [20]. Combining the computed composition profiles with thermodynamic arguments, the authors were able to comment on solidification events taking place in the weld pool. The study on the Fe-Cu binary couple [21] also indicated the possibility of melt undercooling and phase separation in the liquid state.

In this paper, we present the results of laser welding of a Ti/Ni dissimilar couple. This system is distinguished by the following features: (i) Thermo-physical properties of Ti and Ni are widely different (Table I). For example, thermal diffusivity of Ni is much higher than that of Ti at room temperature (roughly three times) and density of liquid Ni is considerably higher than that of liquid Ti (approximately twice). These differences can significantly influence the heat transfer and solutal convection, respectively. (ii) There are three equilibrium intermetallic compounds in the system (Fig. 1) which can form from the liquid through invariant reactions. This opens up alternative solidification pathways that the system can choose from based on local thermodynamic and kinetic constraints.

Earlier efforts to weld Ti and Ni could succeed only to a limited extent [19], the problem reported being weld cracking due to the formation of brittle intermetallics. However, a detailed study of the solidification phenomena which lead to the observed microstructure was not

attempted. Here we report some results on the microstructural evolution in the weld pool and analyse them on the basis of known physical processes occurring during DMW and the thermodynamics of the system. In particular, our results show: (1) the effect of a very steep concentration gradient ahead of the fusion interface in inhibiting the growth of the base metal grains into the melt; (2) the growth of the Ti2Ni phase toward the Ti base metal *along*, and not *opposite* to, the direction of heat removal, demonstrating the interaction of phase diagram considerations with the transport phenomena in the weld pool; and (3) the importance of fluid flow in the melt resulting in the occurrence of titanium dendrites even in the middle of weld pool and the segregation of this lighter phase toward the top surface and that of the heavier NiTi phase toward the bottom.

2. Experiments

Matching surfaces of commercially pure Ni and Ti plates of dimension 8 cm × 4 cm × 2 cm approximately were prepared to a final finish by polishing through 600 grit emery papers. The dissimilar plates were clamped in a butt welding geometry on a computer controlled X-Y table which could be moved relative to the laser source at a constant speed. A continuous wave CO_2 laser operating at 5 kW power with a He shroud as a protective atmosphere was used for welding. The laser was focused to a diameter of approximately 2 mm at the sample and placed symmetrically with respect to the two plates. The relative speed of the laser beam was varied between 500 mm/min to 2 m/min. In all the cases, we could obtain partial penetration welds with no visible macroscopic cracks on the weld surfaces excepting the one welded at the highest speed (2 m/sec). This sample broke after welding due to insufficient penetration. Specimens were cut from these samples and prepared for metallographic observation by grinding and

polishing till 1 μm diamond paste. Differential etching with Kroll's reagent for the Ti side and for the weld pool, and Flat's solution for the Ni side provided sufficient contrast [25]. The prepared samples were observed in a JEOL JSM-840A scanning electron microscope (SEM) equipped with an energy dispersive spectrometer (EDS). Although we have used a range of welding speed and focusing conditions, the generic features of microstructural evolution are similar under these experimental conditions. In this paper, therefore, we report the results for the welding speed of 1 m/min as a representative case. A comparative study concerning of the effect of the welding parameters on the details of microstructural evolution will be communicated elsewhere.

3. Results

3.1. General observations

Different phases constitute the microstructure of the weld pool and they are identified on the basis of composition analyses using EDS. Although errors involved in the measurements preclude very accurate determination of the phase composition, the measurements do help us to identify the phases themselves because the intermetallic compounds in this system occur at widely different compositions (Fig. 1). The terminal solid solutions with variable solute content will henceforth be referred to as (Ti) and (Ni) respectively, and the intermetallic compounds by their respective stoichiometric ratios.

Fig. 2 is a low magnification image of a transverse section of the welded sample. The weld pool is asymmetric with a larger extent of melting taking place in the Ti side. The weld

macrostructure as observed in this image is characterized by a bright band that outlines the fusion interface in the Ti side and large blocks of NiTi toward the bottom half of the pool.

The reason for the asymmetry of the weld pool shape is the lower thermal diffusivity of Ti compared to that of Ni (Table I) which leads to more localized heating and consequently a greater amount of melting of Ti. From Fig. 2, we can also estimate the average composition of the melt by measuring the area of the fusion zones in each base metal and using the molar volume data (Table I). The average composition turns out to be Ti – 41 at% Ni, which falls in the Ti_2Ni+NiTi two-phase region of the Ti-Ni phase diagram (Fig. 1). However, it is an overall estimate, and hence does not rule out any variation of composition (with consequent microstructural variation) that may occur locally. These variations indeed occur, and are presented in the following sub-sections.

3.2 Microstructure near the fusion interfaces

Micrographs in Fig. 3 reveal the finer features of the bright band at the Ti fusion interface. The band is made up of Ti_2Ni dendrites which grow toward the base metal (see Fig. 3(a)). We observe limited growth of cells from the base metal grains into the weld which is stopped by the Ti_2Ni dendrites growing from the opposite direction. The liquid in the interdendritic space solidifies as the Ti+Ti_2Ni eutectic, which is shown in the inset of Fig. 3(a). In Fig. (3(b)), one can observe the Ti_2Ni dendrites form in the weld pool at some distance ahead of the fusion interface. Fig. 3(c) shows the EDS spectrum obtained from a Ti_2Ni dendrite. The corresponding composition analysis is shown in the inset.

Fig. 4 shows the fusion interface at the Ni side. At the interface, we see three bands running parallel to the interface. These are marked ‘A’, ‘B’, and ‘C’ in Fig. 4(a). The grains of the base

metal do not grow into the weld; instead, solidification starts with the formation of a layer of (Ni) solid solution on the base metal grains of pure Ni (Fig 4(b)). This is followed by the formation of the intermetallic compound Ni_3Ti, which wets the (Ni) layer. Contrary to the expectation from the phase diagram of the system, a two phase region of Ni_3Ti + (Ni) is not observed between these two layers which constitute the band 'A'. However, a Ni_3Ti + NiTi eutectic microstructure can be seen in the band 'B' (Fig. 4(c)). In addition to this eutectic, faceted primary Ni_3Ti dendrites are also observed in this band. Band 'C' consists of a layer of NiTi which exhibits cellular growth both toward the band 'B' and into the weld pool.

The sequence of formation of these bands at the Ni interface (Fig. 4), as well as the Ti_2Ni band at the Ti interface (Fig. 3), is discussed in Section 4.1 invoking an interplay of the nature of the phase diagram of the Ti-Ni system and process induced transport phenomena in the weld pool.

3.3. Microstructure in the middle of the weld

Microstructure in the central region of the weld pool consists mostly of NiTi and Ti_2Ni.

Fig. 5(a) shows a typical microstructure of this region. Composition analysis identifies the dendrites with light gray contrast to be NiTi and the dark gray regions to be Ti2Ni. We can also see fine (Ti) dendrites inside the coarse NiTi dendrites. Some of these (Ti) dendrites grow to a greater extent, as evident in the back-scattered electron (BSE) image in Fig. 5(b). In this micrograph, we see the coarser NiTi structure to be built around the finer (Ti) dendritic core.

Throughout the central part of the weld, frequently alternate layers of coarse and fine NiTi form. Fig. 6 shows a BSE image where a layer of coarse, equiaxed NiTi dendrites is sandwiched between layers containing fine NiTi particles, while the Ti_2Ni phase has grown across the layers.

NiTi also occurs as large segregated regions in the bottom half of the weld pool (Fig. 7). In Fig. 7, the large, dark, crescent shaped features belong to the NiTi phase, which have grown without any resolvable sub-structure. NiTi also forms with cellular/dendritic morphology that accounts for the remaining microstructural features with bright contrast of this figure. Cellular breakdown from the periphery of the massive NiTi blocks is shown in the inset.

As we move from the bottom half of the weld pool toward the top, the (Ti) dendrites appear more frequently. Fig. 8(a) is a typical top view micrograph of the central region of the weld. This figure reveals (Ti) dendrites surrounded by Ti_2Ni dendrites, which is demonstrated more clearly in the BSE image of Fig. 8(b). Presence of Ti+Ti_2Ni eutectic in the interdendritic regions of these faceted Ti_2Ni dendrites can also be observed.

These microstructures (Figs. 5-8) suggest the important role played by the fluid flow in the melt which is further discussed in Section 4.2.

4. Discussion

4.1 Microstructure near the fusion interfaces

In contrast to SMW, the growth of the base metal grains into the weld pool is inhibited during dissimilar welding (Figs. 3(a) , 4(a)) owing to the presence of the steep composition gradient ahead of the interface. Additionally, our observations indicate that Ti_2Ni dendrites at the Ti fusion interface grow toward the base metal along the heat extraction direction (Fig. 3). This observation is counter-intuitive, because, in welding, growth of the solid phase at the fusion interface normally takes place opposite to the direction of heat removal and is constrained by the

rate of the movement of the isotherms. Growth along a negative temperature gradient is also observed at the Ni fusion interface where NiTi cells (band 'C' in Fig. 4(c)) grow into the band 'B'. In the following sub-sections, we rationalize these observations by considering the interaction of the phase diagram of the system with the transport processes in the weld pool.

4.1.1. Formation of the Ti_2Ni band at the Ti interface

Fig. 9 presents a schematic illustration of the temperature and composition profiles near the fusion interface in Ti. In this diagram, a monotonic and linear temperature variation is assumed to reflect the heat extraction through the cooler base metal. The composition profile, however, is assumed to be steep in the stagnant boundary layer where mixing can take place only through atomic diffusion. Beyond this layer, advective mixing makes the composition variation smoother. We also draw in the figure the liquidus temperature profiles of different phases corresponding to the assumed variation of composition. Regions in the figure where the actual melt temperature is lower than the liquidus temperature of a phase define the thermodynamically permissible range of existence for that phase.

We see from the figure (Fig. 9) that (Ti) can grow from the fusion interface at the Ti side and we do observe titanium cells growing into the weld pool in Fig. 3(a). However, growth of columnar (Ti) dendrites is not observed in this figure. We believe that (Ti) dendrites did form, but they were detached/fragmented and flown into the middle of the weld pool by the convective currents (see Section 4.2.1). Following the permissible extent of the (Ti) phase in Fig. 9, there appears a region in space where no solid phase can exist at the given instant. This is followed by the region where Ti_2Ni formation is possible. NiTi can form farther into the pool when the composition becomes favourable. Because of the steeper slope of the NiTi liquidus line compared to that of

Ti_2Ni (Fig. 1), the driving force for NiTi formation will exceed that for Ti_2Ni. Hence NiTi will nucleate first from the liquid, and Ti_2Ni is most likely to form heterogeneously on it through a peritectic reaction. Once formed, it is easier for the Ti_2Ni to grow toward the base metal down the thermal gradient, giving rise to the observed microstructure (Fig. 3).

4.1.2. Formation of bands near the Ni interface

Formation of the bands (marked 'A', 'B' and 'C' in Fig. 4) at the Ni fusion interface can be understood in a similar manner. We see from Fig. 10 that solidification can start with the formation of (Ni). It also shows a region where the (Ni)+Ni_3Ti eutectic can form after the (Ni) phase field. However, this eutectic is not observed in the weld pool; instead, we find in Fig. 4(b) that a layer of Ni_3Ti that has grown over the existing (Ni) layer in preference to a coupled growth of (Ni)+Ni_3Ti eutectic. Fig. 10 predicts NiTi to be the next phase to solidify, but it can form only at some distance ahead of the Ni_3Ti layer, leaving the region marked 'B' in Fig. 4(a) still in the liquid state. This happens because of the relatively lower invariant temperature of the Ni_3Ti+NiTi eutectic compared to the congruent freezing temperatures of Ni_3Ti and NiTi (Fig. 1). Growth of NiTi cells from band 'C' into the band 'B' (Fig. 4(c)) supports this construction. The region 'B' solidifies later as the Ni_3Ti+NiTi eutectic.

4.2. Microstructure in the middle of the weld

As noted in Section 3.1, the average composition of the melt corresponds to the Ti_2Ni+NiTi two-phase region of the phase diagram, and these two phases do indeed constitute the microstructure in the central region of the weld. This reflects the well mixed nature of the melt over macroscopic length scales. However, local variations in the microstructure such as (Ti) dendrites

surrounded by NiTi dendrites, appearance of alternate layers of coarse and fine NiTi, macrosegregation of NiTi blocks toward the bottom and that of (Ti) toward the top surface of the weld, are also observed. These are discussed below.

4.2.1. (Ti) dendrites in the middle

Some of the NiTi dendrites are observed to grow surrounding finer (Ti) dendrites (Fig. 5). It is unlikely that these (Ti) dendrites nucleated in the central region where the melt contained high solute concentration. Instead, the more probable situation is that they nucleate near the Ti interface where the melt is Ti-rich, or the cells/dendrites advancing from the base Ti get fragmented due to the fluid flow, and these are then flown away into the weld pool by the convective currents. Since the Ti-rich solid solution phase has the highest liquidus temperature among all the phases, it can flow freely toward the fully liquid central region without hindrance from any solid phase. NiTi can nucleate heterogeneously on this (Ti) phase and grow surrounding them (Fig. 5).

4.2.2. Alternate layers of coarse and fine NiTi

Equiaxed growth of the NiTi resembles unconstrained dendritic growth in an undercooled melt. However, a strong fluid flow is expected to make the advective heat and species transfer to dominate over atomic transport processes, and consequently influence the growth the NiTi phase. The observation of alternate coarse and fine layers NiTi (Fig. 6) gives evidence for such effects of fluid flow in bringing about periodic fluctuations in local composition/temperature. A similar kind of alternating microstructural feature, termed as low velocity banding, has often been observed during laser processing of materials [26] and is believed to originate from

convective instabilities [27]. However, we note that although convection is the most likely reason behind the present observation, one cannot rule out the possibility of a peritectic banding [27] involving NiTi and Ti_2Ni.

4.2.3. Macrosegregation in the weld

Fluid flow effects are also manifested at another level through a macrosegregation pattern caused by a density gradient in the liquid. As noted in Section 1, the density difference between liquid Ti and liquid Ni can give rise to a solutal natural convection. The relative strength of this flow compared to the Marangoni convection can be estimated by computing the dimensionless solutal Rayleigh (Ra_s) number and Marangoni (Ma) number respectively [27]. As shown in Appendix, Ra_s turns out to be five times that of Ma for the present case. This indicates a very important role played by the solutal convection, which is supported by the experimental observation of the segregation of the lighter (Ti) and Ti_2Ni phases toward the top surface (Fig. 8(a)) and that of heavier NiTi blocks toward the bottom half of the pool (Fig. 7). We note that similar kind of segregation patterns have also been observed during laser surface alloying of Zn with Al where the component liquids had significant difference in density [28].

4.2.4 Solidification sequence

Fig. 11 summarizes schematically the sequence of the phase evolution in the Ti Ni weld pool which explains the current observations. The schematic snapshots depict the solidification events in the weld pool with increasing time (from ***t1*** till ***t6***) as we move from the top toward the bottom of the figure. In brief, these events are:

t1: Solidification starts from both the base metal sides with the formation of the terminal solid solutions.

t2: Ni_3Ti layer forms on the (Ni) at the Ni side. Ti side shows the formation of cells and dendrites at the growing solidification interface.

t3: (Ti) cells and dendrites are detached and flown away into the middle of the pool. Ni side develops a NiTi layer parallel to, but at some distance ahead of, the Ni_3Ti layer that had formed at *t2*. Some NiTi also starts to segregate toward bottom.

t4: The Ni_3Ti+NiTi eutectic forms between the Ni_3Ti and NiTi layers at the Ni side. The NiTi block at the bottom grows. Equi-axed NiTi dendrites grow at different locations in the weld pool.

t5: More NiTi nucleate and grow in the middle of the pool. Ti_2Ni forms surrounding the NiTi at favourably located regions.

t6: Ti_2Ni dendrites grow toward the Ti base metal near the Ti fusion interface; interdendritic space solidifies as the Ti+Ti_2Ni eutectic. Rest of the weld solidifies with further growth of Ti_2Ni and NiTi.

5. Conclusions

We have presented a study of microstructural evolution in the fusion zone of a laser welded dissimilar binary couple of Ti/Ni. Based on our study, we draw the following conclusions:

1. The difference in the properties lead to a marked asymmetry in the macroscopic shape of the weld pool.

2. At the fusion interfaces, continuous growth of the base metal grains into the weld is either absent or very limited.

3. Change in microstructure is most drastic near the interfaces, and comparatively less so away from the interfaces.

4. Fluid flow caused by the density difference of the components results in a macrosegregation in the weld.

5. Fluid flow is also effective in carrying (Ti) dendrites over large distances in the pool.

6. There is significant undercooling of the compositionally inhomogeneous melt. It is evidenced by the growth of the Ti2Ni dendrites toward the Ti interface, the equiaxed NiTi in the middle of the pool, and the NiTi cells toward the Ni interface.

7. Microstructural observations are rationalised by considering the interaction of the thermodynamics of the system with the transport phenomena in the weld pool.

Acknowledgements

One of the authors (KC) wishes to thank Dr. R. Galun, TU Clausthal, Germany, for his kind hospitality during the author's stay and his help with the laser welding experiments. The financial support form DRDO, Govt. of India is gratefully acknowledged.

References

1. S.A. DAVID, S.S. BABU and J.M. VITEK, *JOM* **55** (2003) 50.

2. J.N. DUPONT, S.W. BANOVIC and A.R. MARDER, *Welding Journal* **82** (2003) 125-s.

3. T.W. NELSON, J.C. LIPPOLD and M.J. MILLS, *Welding Journal* **79** (2000) 267-s.

4. M. SIREESHA, V. SHANKAR, K.A. SHAJU and S. SUNDARESAN, *Mater. Sci. Eng.* **A292** (2000) 74.

5. M.D. ROWE, T.W. NELSON and J.C. LIPPOLD, *Welding* Journal **78** (1999) 31-s.

6. T.W. NELSON, J.C. LIPPOLD and M.J. MILLS, *Welding Journal* **78** (1999) 329-s.

7. A.A. OMAR, *Welding Journal* **77** (1998) 86-s.

8. E.J. BARNHOUSE and J.C. LIPPOLD, *Welding Journal* **77** (1998) 477-s.

9. C. PAN and Z. ZHANG, *Materials Characterization* **36** (1996) 5.

10. Z. SUN and T. MOISIO, *J. Mater. Sci. Lett.* **13** (1994) 802.

11. Z. SUN and T. MOISIO, *Mater. Sci. Tech.* **9** (1993) 603.

12. H.K.D.H. BHADESHIA, S.A. DAVID and J.M. VITEK, *Mater. Sci. Tech.* **7** (1991) 50.

13. T.A. MAI and A.C. SPOWAGE, *Mater. Sci. Eng.* **A374** (2004) 224.

14. T. LUIJENDIJK, *J. Mater. Proc. Tech.* **103** (2000) 29.

15. B. MAJUMDAR, R. GALUN, A. WEISHEIT and B.L. MORDIKE, *J. Mater. Sci.* **32** (1997) 6191.

16. Z. SUN and R. KARPPI, *J. Mater. Proc. Tech.* **59** (1996) 257.

17. Z. SUN and J.C. ION, *J. Mater. Sci.* **30** (1995) 4205.

18. P.S. LIU, W.A. BAESLACK and J. HURLEY, *Welding Journal* **73** (1994) 175-s.

19. J. SERETSKY and E.R. RYBA, *Welding Journal* **55** (1076) 208-s.

20. G. PHANIKUMAR and K. CHATTOPADHYAY, *Sci. Tech. Weld. Join.* (2005).

21. G. PHANIKUMAR, S. MANJINI, P. DUTTA, J. MAZUMDAR and K. CHATTOPADHYAY, *Met. Mater. Trans.* (in press).

22. G.PHANIKUMAR, P. DUTTA and K. CHATTOPADHYAY, *Met. Mater. Trans.* **35B** (2004) 339.

23. P.S. WEI and F.K. CHUNG, *Met. Mater. Trans.* **31B** (2000) 1387.

24. “Smithels Reference Book", Editors: E.A. BRANDES and G.B. BROOK (7th Edition, Butterworth-Heinemann, Oxford, MA, 1992) p. 1040.

25. G.F. VANDER VOORT in “Metallography: Principles and Practice" (Mc-Graw Hill Book Company, 1984).

26. M. GREMAUD, M. CARRARD and W. KURZ, *Acta Mater.* **38** (1990) 2587.

27. W. KURZ and R. TRIVEDI, *Met. Mater. Trans.* **27A** (1996) 625.

28. P.A. CARVALHO, A.M. DEUS, R. COLACO and R. VILLER, *Acta Mater.* **46** (1998) 1781.

29. J.H. FERZIGER and M. PERIC in “Computational Methods for Fluid Dynamics” (3rd Edition, Springer, 2002), pp. 372-382.

Appendix

Expressions for Ra_s and Ma

We can compute the solutal Rayleigh number Ra_s and the Marangoni number Ma by modifying the expressions given in [29] as:

$$Ra_s = \frac{g\Delta\rho L^3}{\mu\kappa},$$

$$Ma = -\gamma_T \frac{dT}{dx}\frac{L^2}{\mu\kappa},$$

where g is the acceleration due to gravity, $\Delta\rho$ is the density change involved, L is the characteristic lengthscale, μ is the liquid viscosity, κ is the thermal diffusivity, γ_T is the temperature coefficient of surface tension, and $\frac{dT}{dx}$ is the temperature gradient. For the present case, we have taken L = weld pool width ≈ 5 mm, $\frac{dT}{dx}$ = typical temperature gradient in the weld pool $\approx 10^5$ Km^{-1}, and $\Delta\rho$ = density difference between the liquid base metals. Using these values, and with other values listed in Table I, we find that $Ra_s = 3.83\times10^4$ and $Ma = 7.8\times10^3$, and hence $Ra_s/Ma \approx 5$.

Table I: Thermo-physical properties of the base metals (after [24])

Property	Ti	Ni
Thermal conductivity ($Wm^{-1}K^{-1}$)	21.6	88.5
Density of solid ($kg\ m^{-3}$)	4500	8900
Density of liquid (kgm^{-3})	4110	7905
Molar volume (m^3mole^{-1})	11.64×10^{-6}	7.43×10^{-6}
Specific Heat ($Jkg^{-1}K^{-1}$)	528	452
Temperature coefficient of surface tension, γ_T ($mNm^{-1}K^{-1}$)	-0.26	-0.38
Viscosity ($mNsm^{-2}$)	5.2	4.9
Enthalpy of fusion ($kJmol^{-1}$)	17.5	17.16

List of Figures

Figure 6	BSE image showing alternate layers of coarse and fine NiTi structures which appear throughout the central region of the weld. Ti_2Ni phase is spread across these layers.
Figure 7	Large NiTi blocks appear mostly near the bottom of the weld pool. Cellular growth from the periphery of the blocky NiTi is shown in the inset.
Figure 8	(a) A top view of the weld pool showing preferential occurrence of the (Ti) dendrites near the top surface of the weld.
	(b) BSE image showing faceted Ti_2Ni surrounding (Ti) dendrites.
Figure 9	Schematic illustration of the variation of temperature, composition and liquidus temperature near Ti fusion interface. Firm lines represent the temperature and composition in the melt and the dashed lines are for the liquidus temperatures of the respective phases (indicated in the figure).
Figure10	Schematic illustration of the variation of temperature, composition and liquidus temperature near Ni fusion interface.
Figure 11	A schematic diagram depicting the evolution of different phases during the solidification of molten weld pool obtained during the laser welding of Ti and Ni. The snapshots at increasing times are presented from top toward bottom. Colormaps indicate the phases. See text for details.

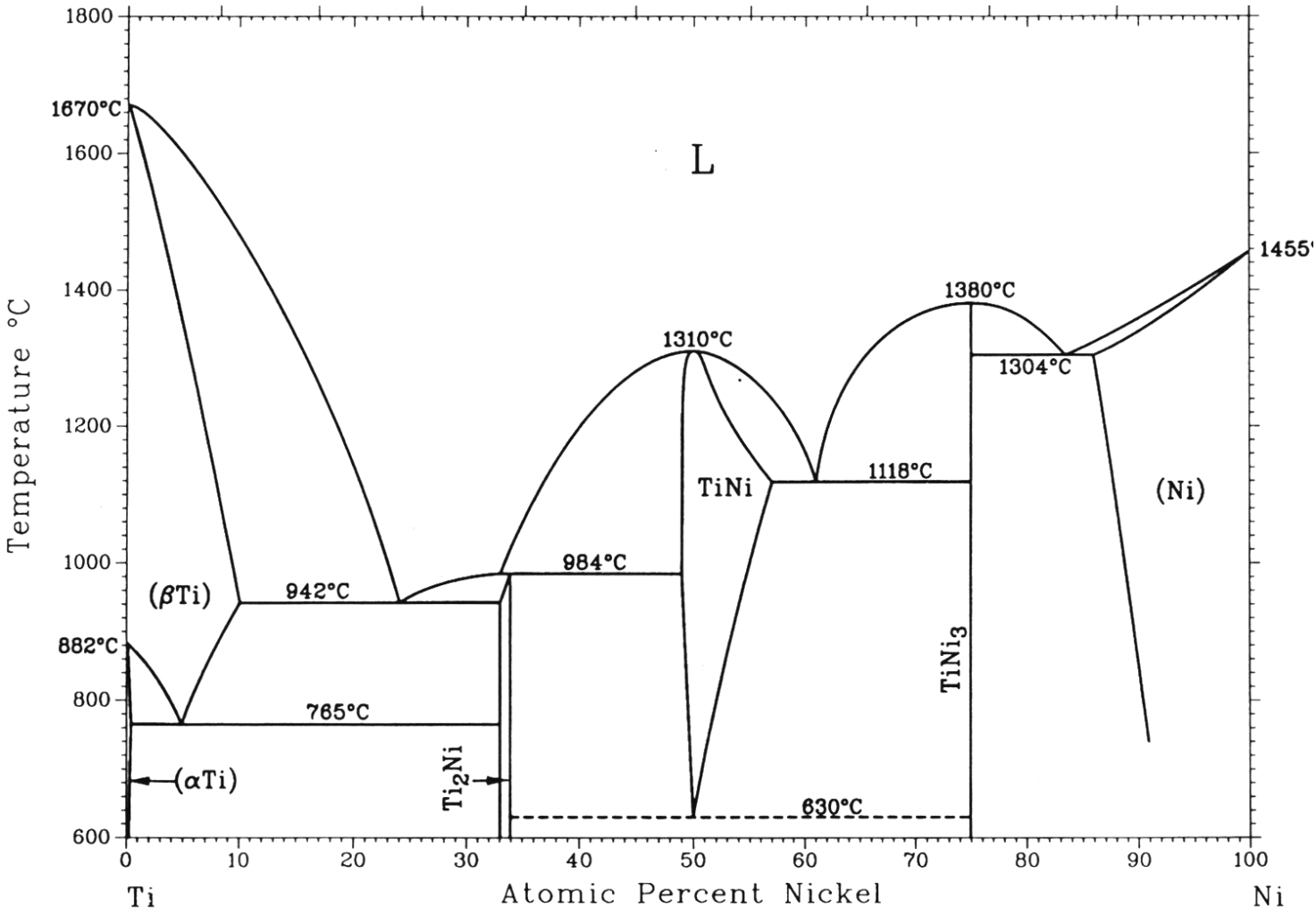
1800
1670°C
1600
1400
1200
1000
882°C
800
600
Temperature °C
L
1455
1380°C
1310°C
1304°C
1118°C
TiNi
(Ni)
984°C
(βTi)
942°C
765°C
(αTi)
Ti2Ni
TiNi3
630°C
0
10
20
30
40
50
60
70
80
90
100
Ti
Atomic Percent Nickel
Ni

Figure 1

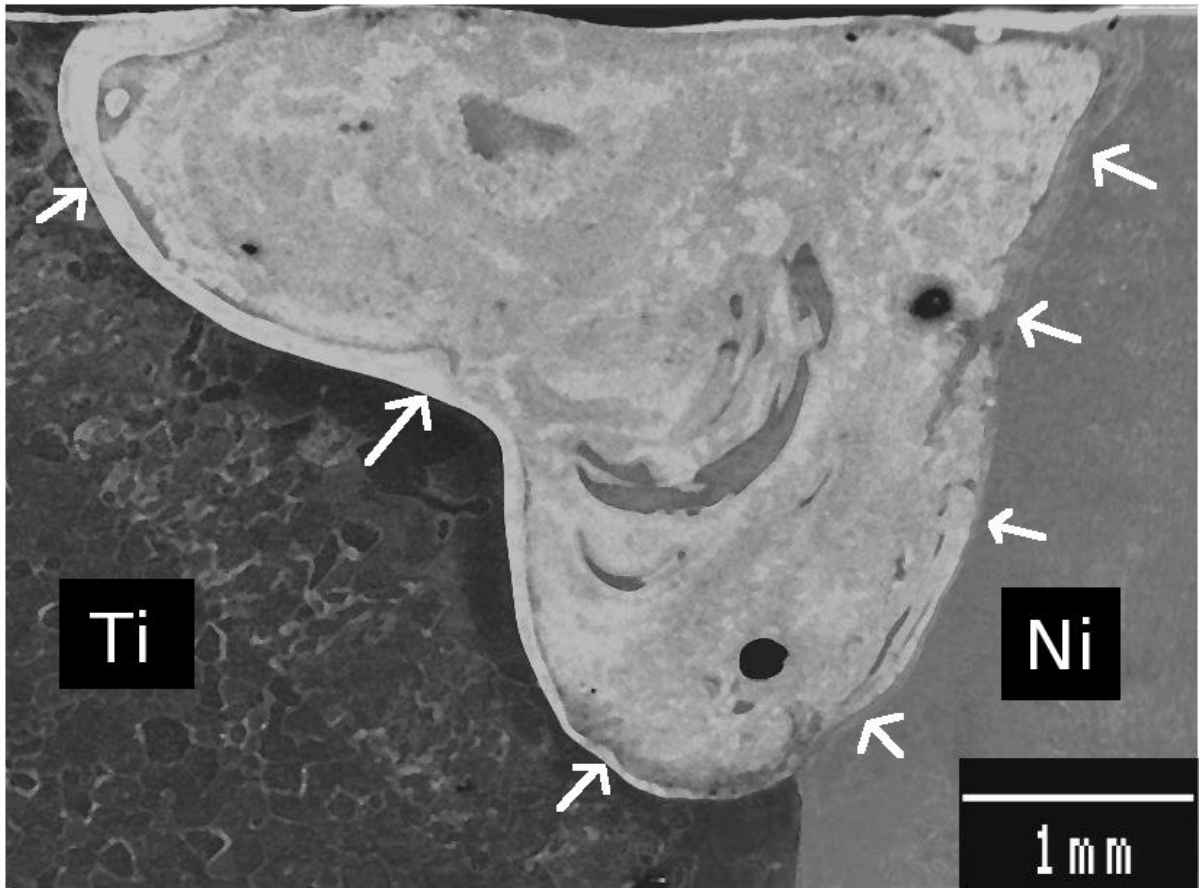

Figure 2

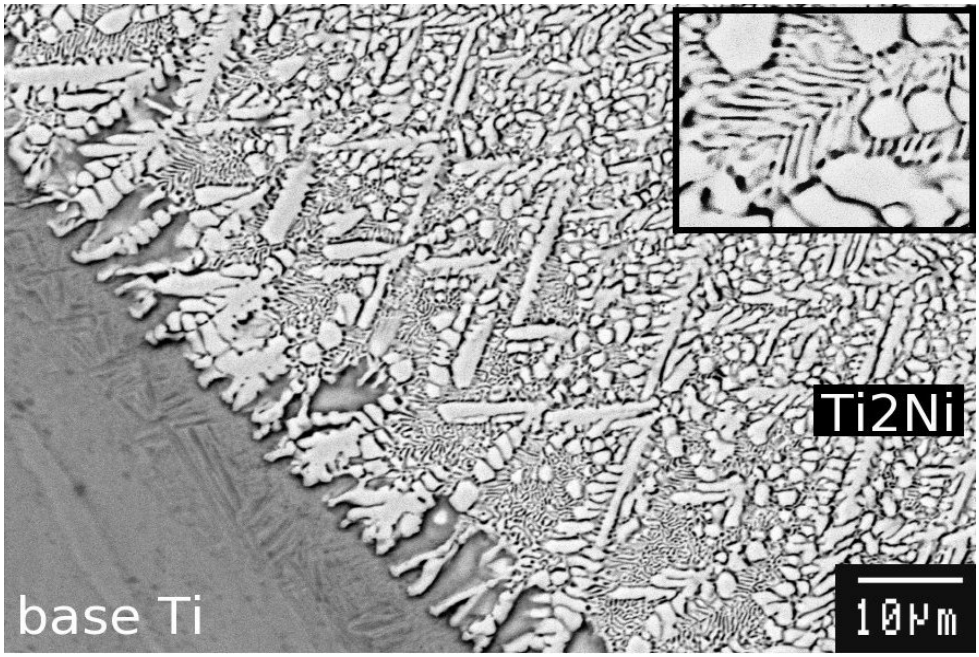

(a)

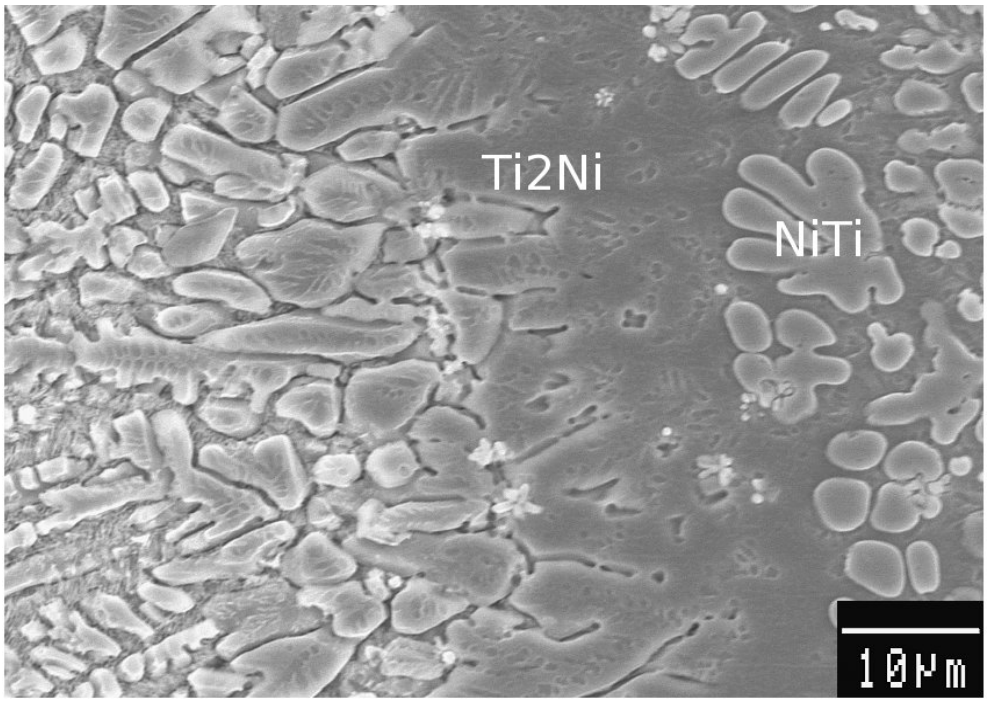

Ti fusion interface ← → weld pool

(b)

Figure 3 …

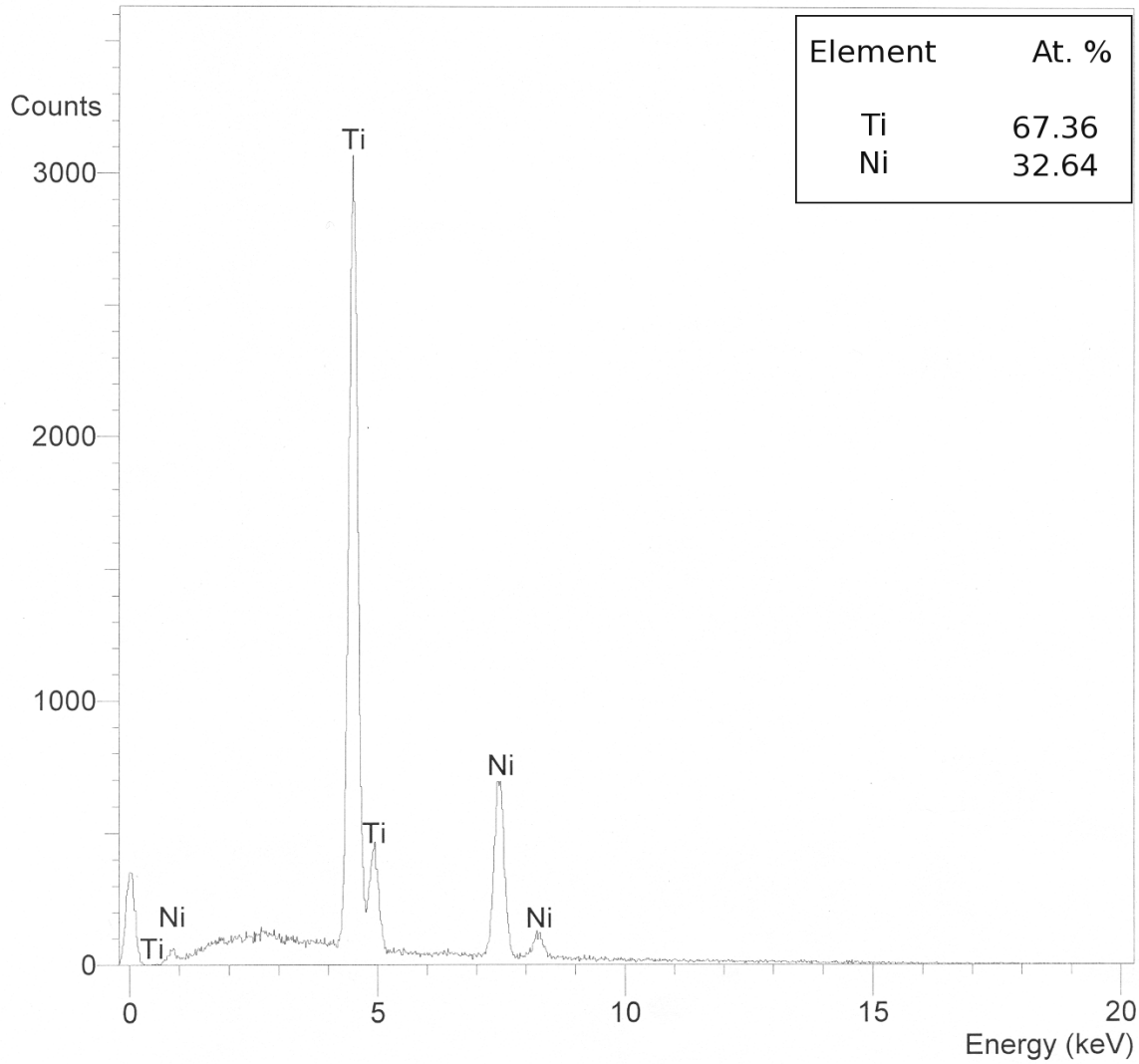
Element At. %
Ti 67.36
Ni 32.64
Counts
3000
2000
1000
0
Ti
Ni
Ti
Ni
Ni
Ti
0
5
10
15
20
Energy (keV)

(c)

Figure 3

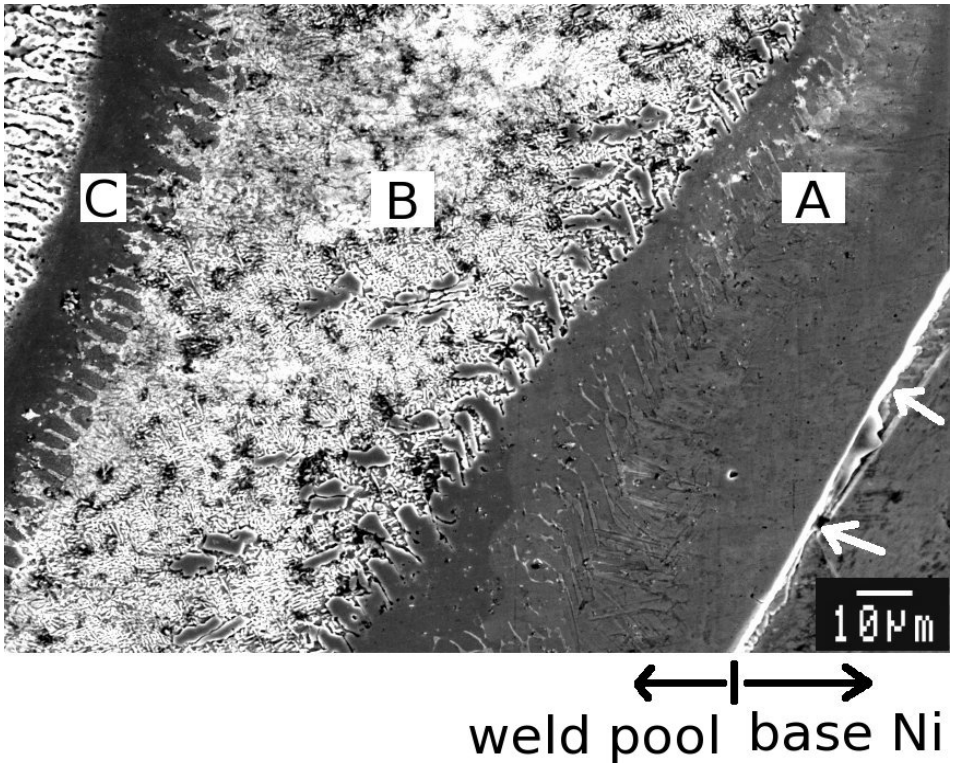

(a)

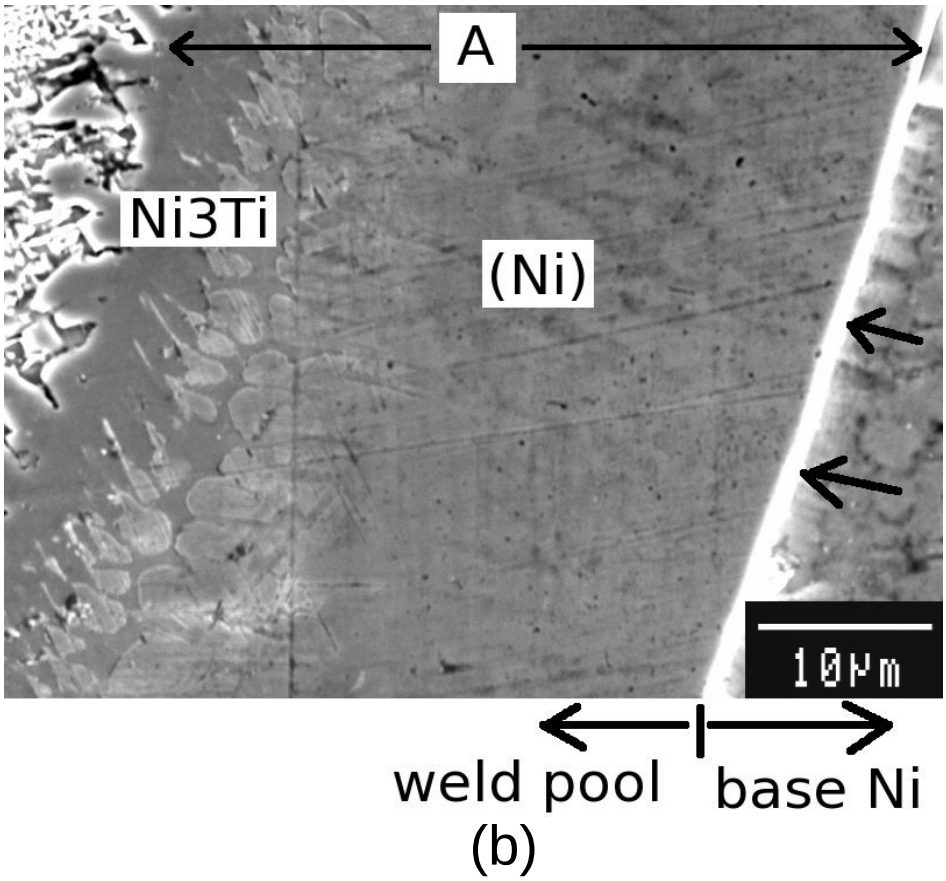

(b)

Figure 4 …

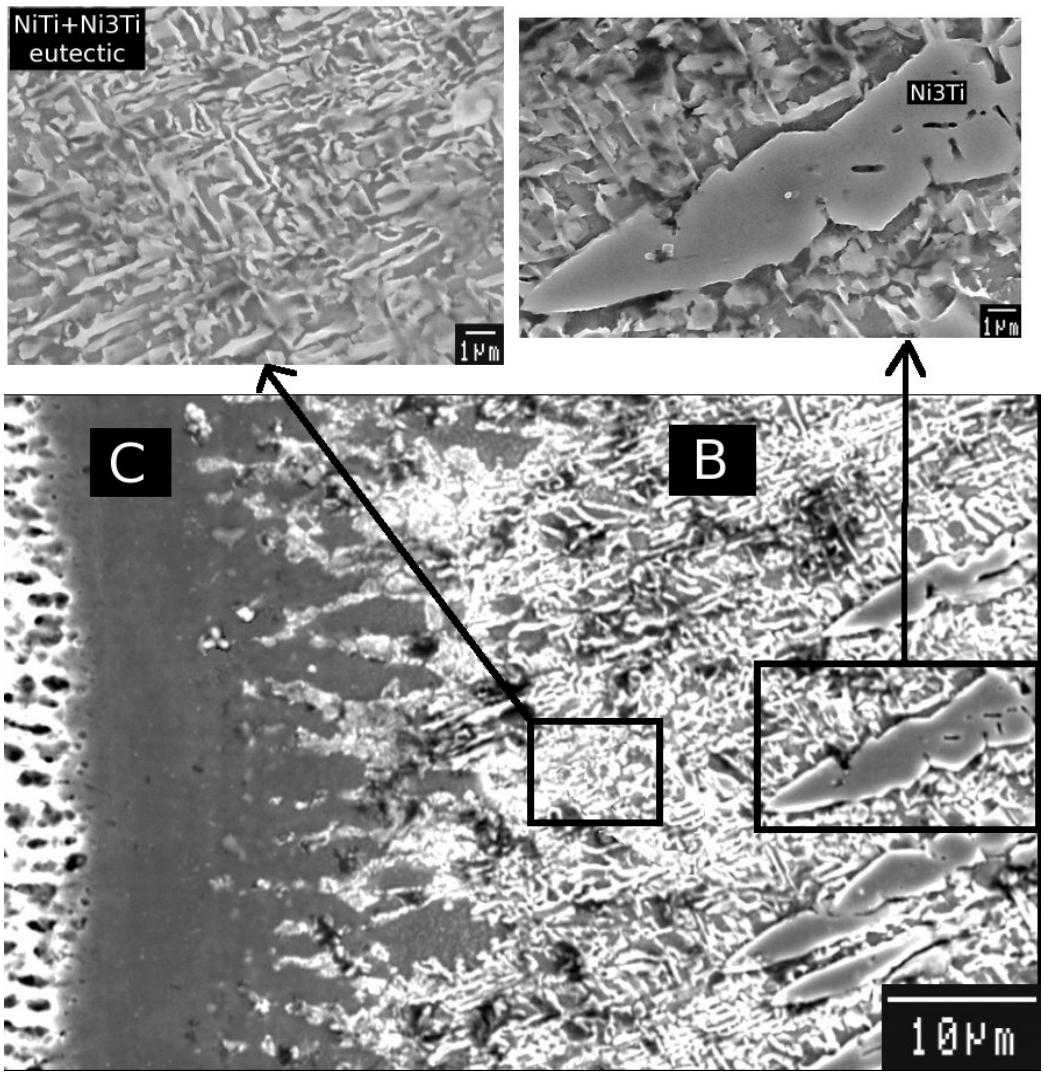

(c)

Figure 4

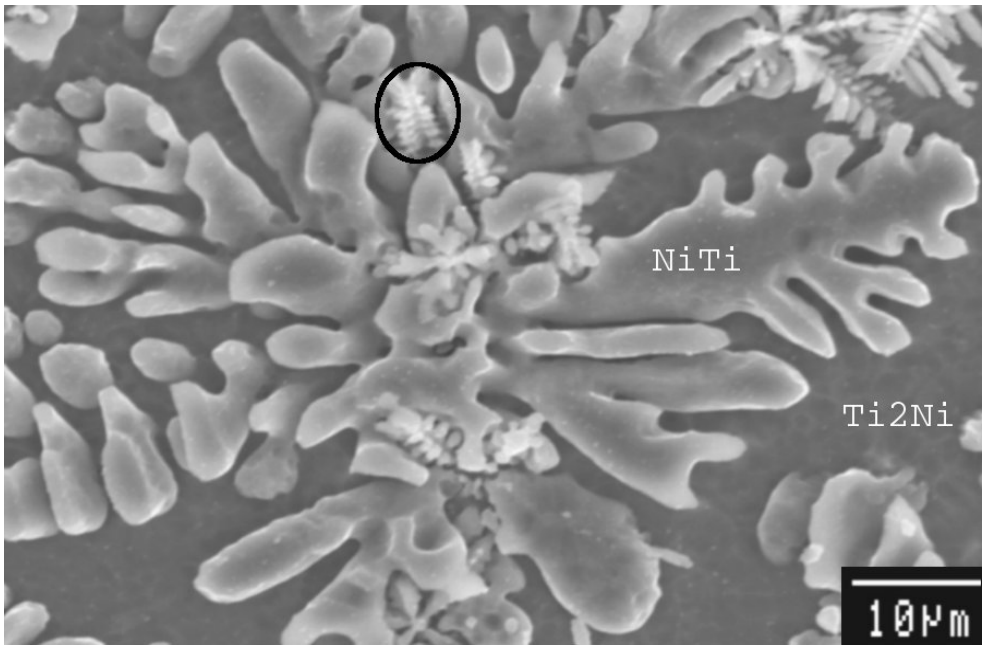

(a)

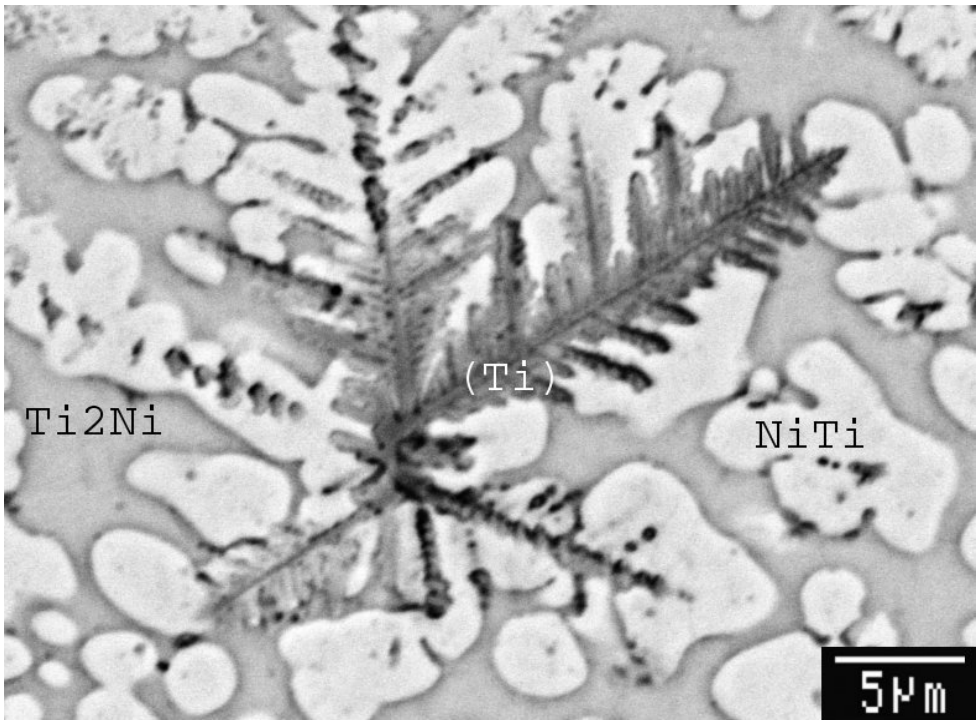

(b)

Figure 5

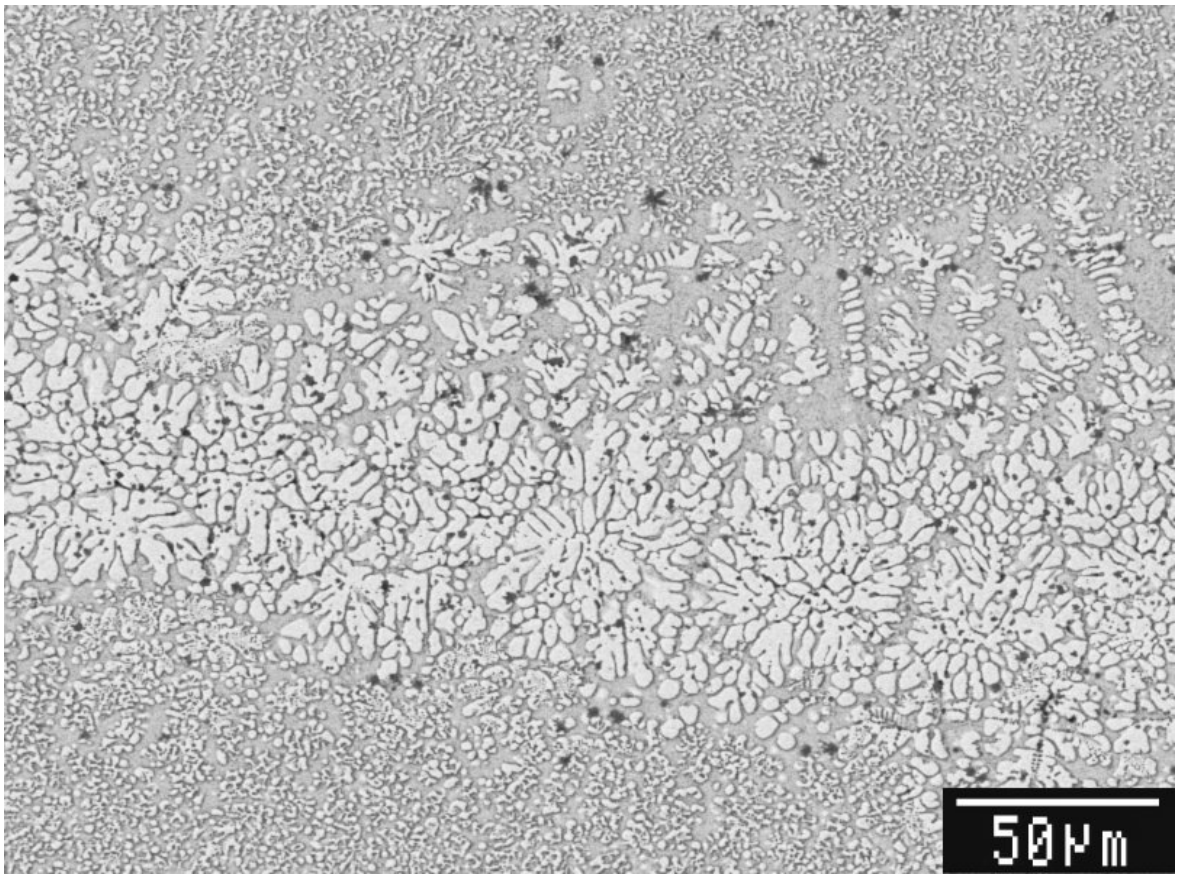

Figure 6

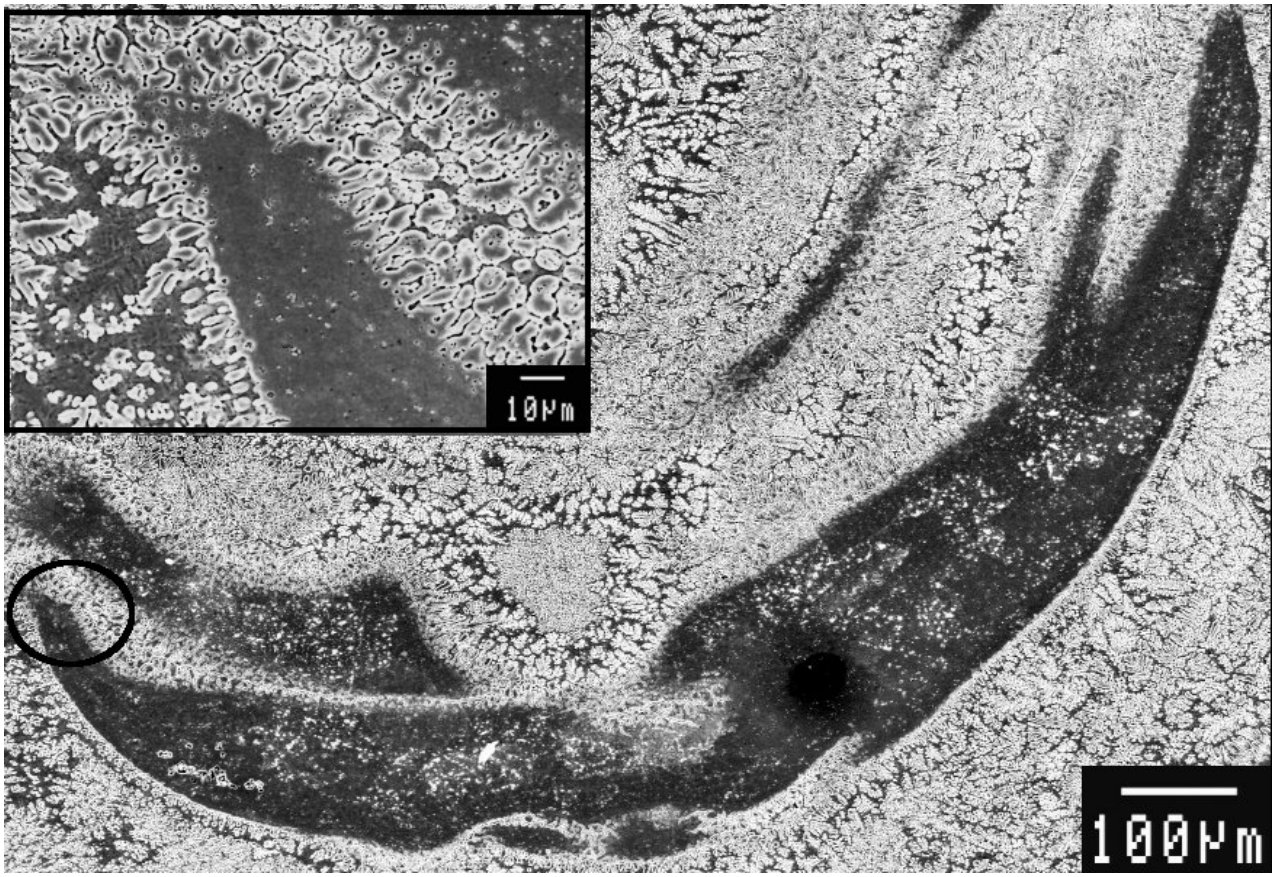

Figure 7

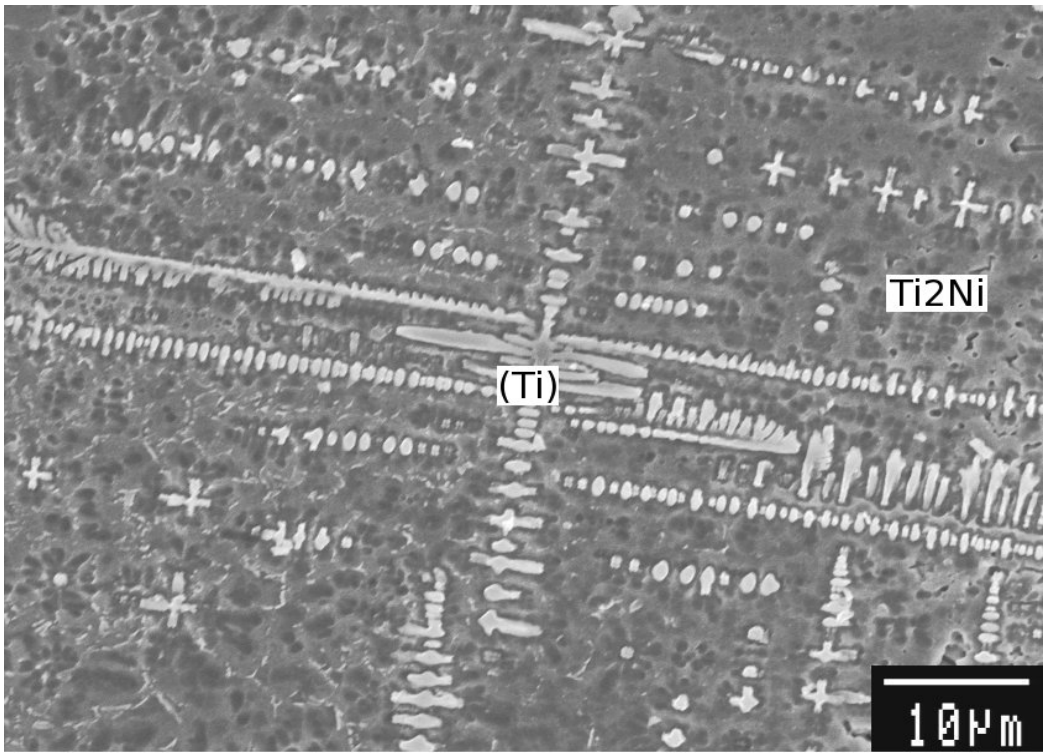

(a)

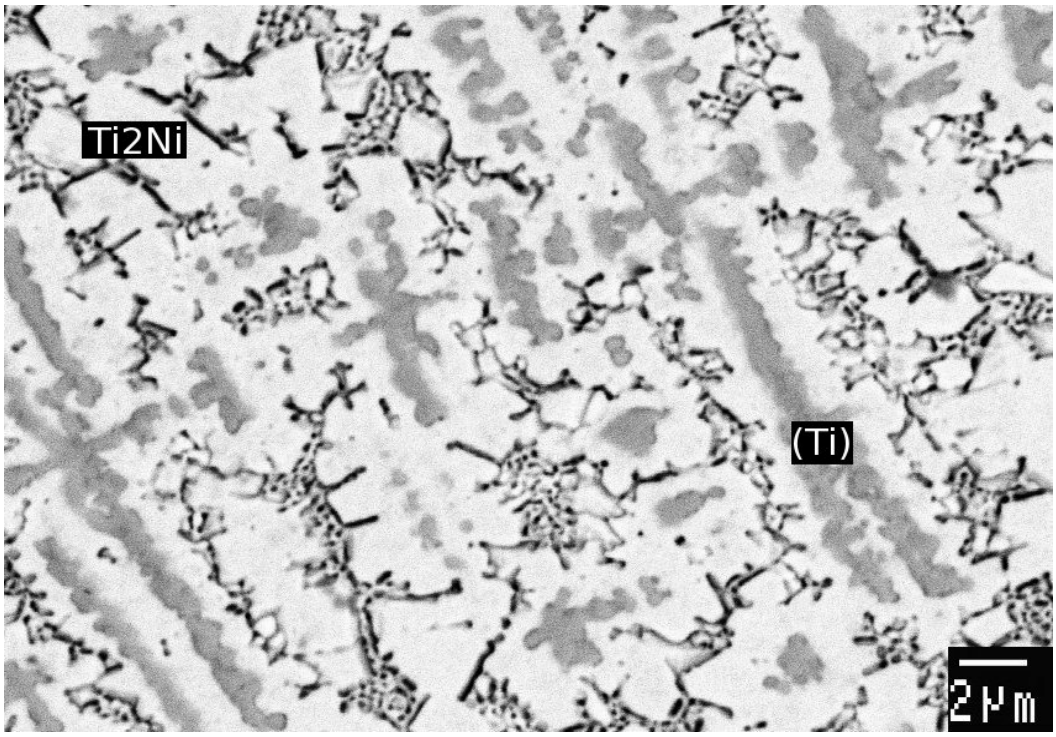

(b)

Figure 8

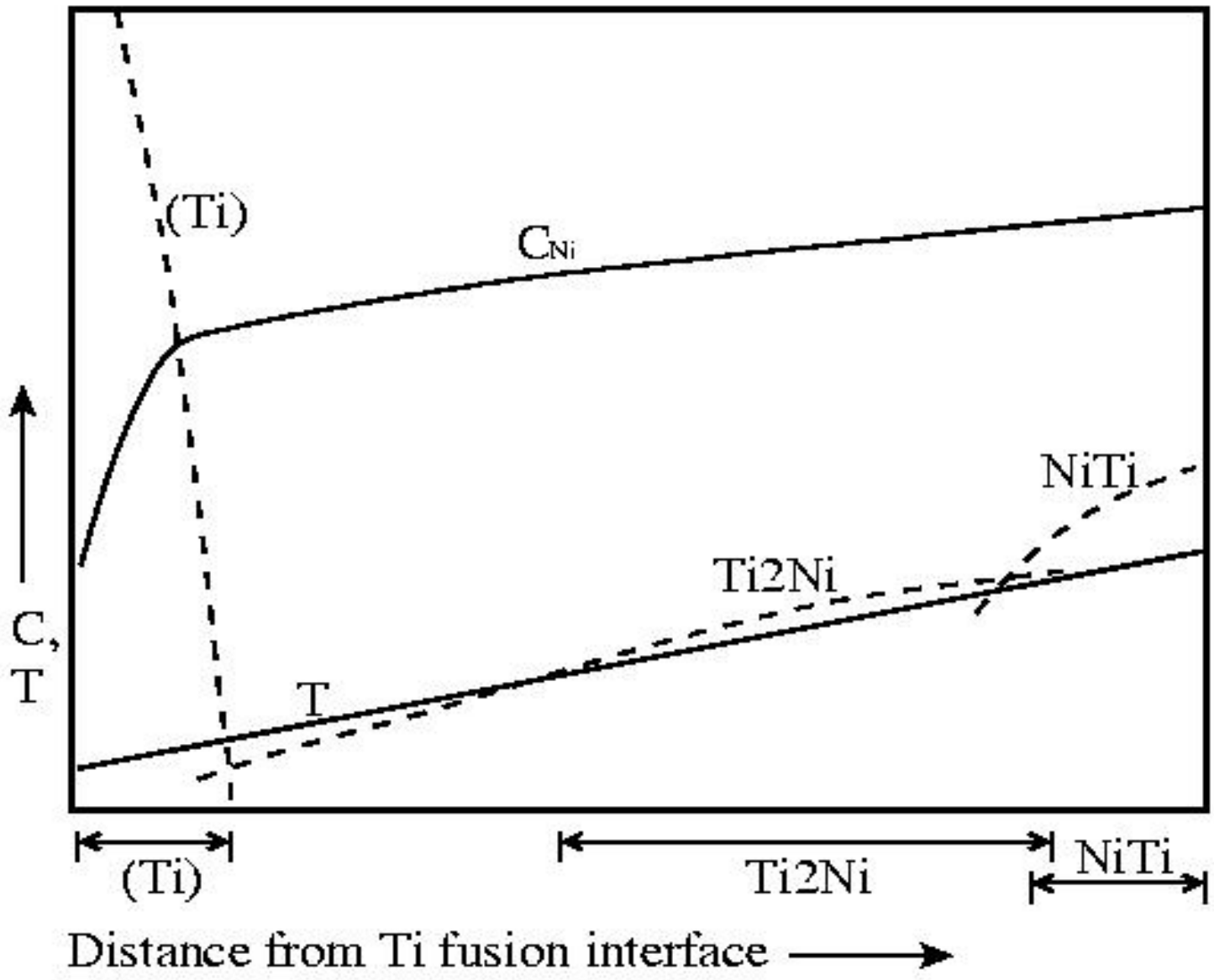
(Ti)
C_{Ni}
NiTi
Ti2Ni
C, T
T
(Ti)
Ti2Ni
NiTi
Distance from Ti fusion interface

Figure 9

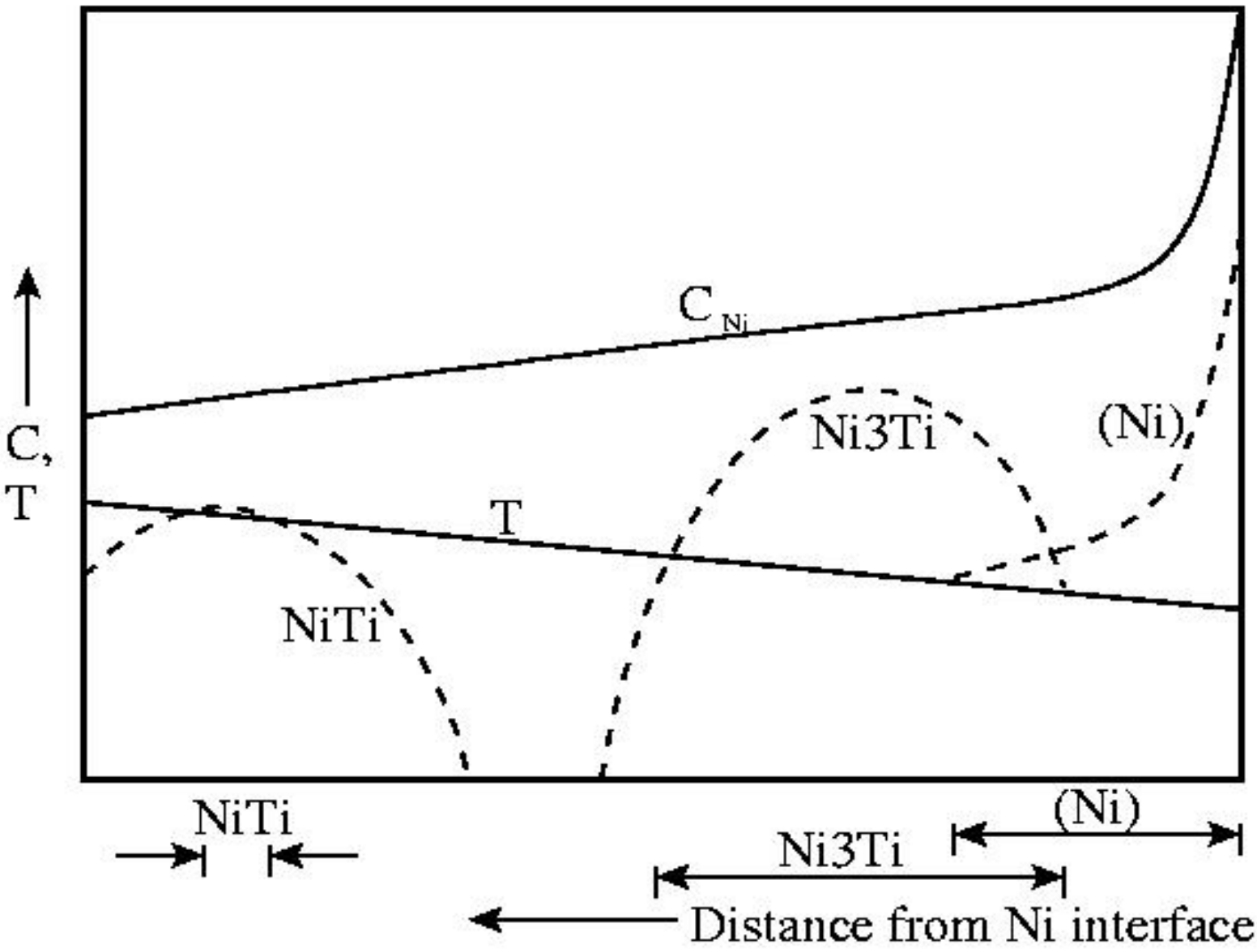
C,
T
C Ni
Ni3Ti
(Ni)
T
NiTi
NiTi
(Ni)
Ni3Ti
Distance from Ni interface

Figure 10

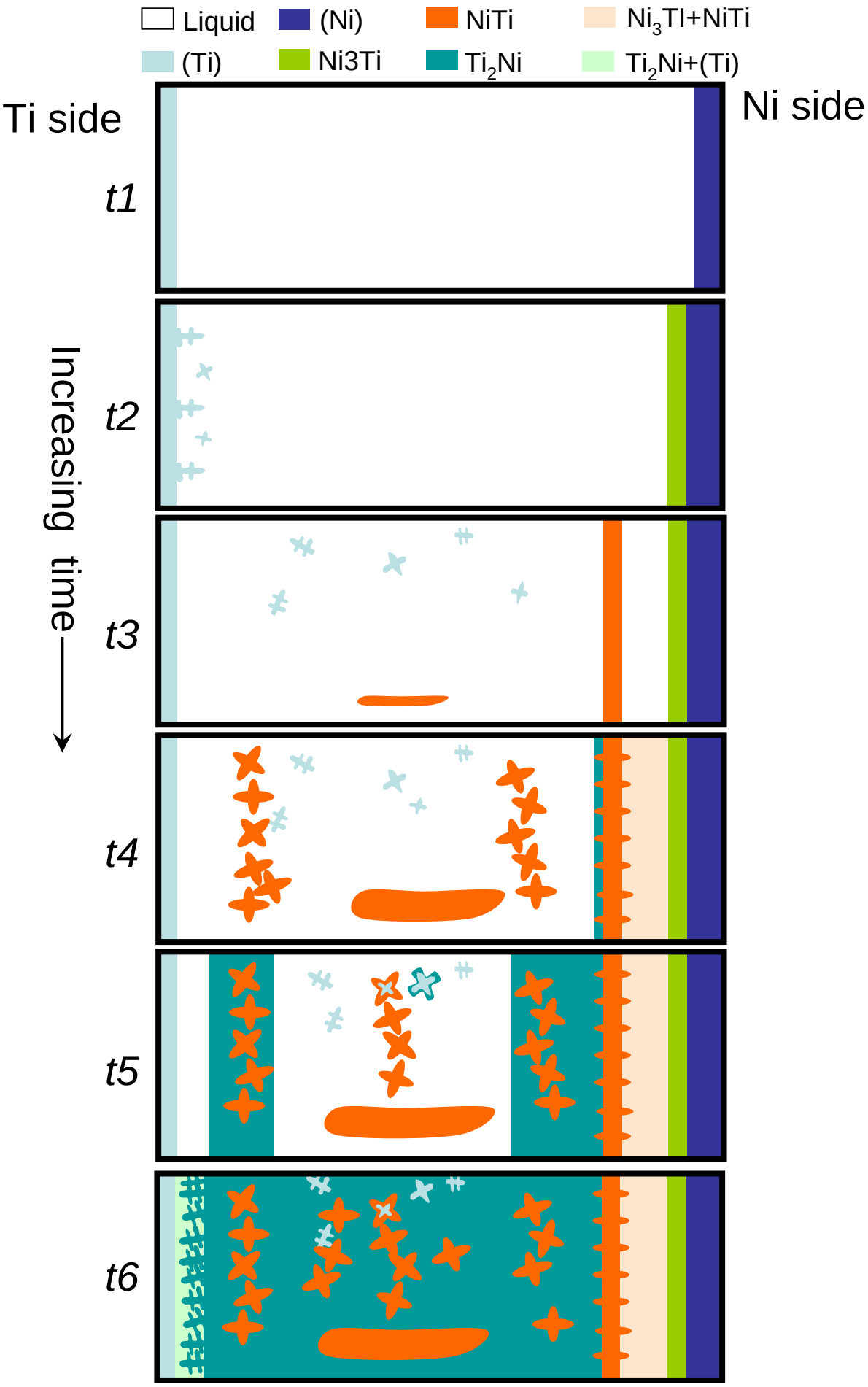
Liquid
(Ni)
NiTi
Ni3TI+NiTi
(Ti)
Ni3Ti
Ti2Ni
Ti2Ni+(Ti)
Ti side
Ni side
t1
t2
t3
t4
t5
t6
Increasing time

Figure 11